Global and Planetary Change
April 2024, Volume 235, Pages 104399 (10p.)
https://doi.org/10.1016/j.gloplacha.2024.104399
https://archimer.ifremer.fr/doc/00881/99285/

Contrasted changes of sea-surface salinity in the southern and northern Okinawa Trough since the mid-Holocene

Li Dongling [1, 2], Wu Yanjuan [1, 2], Seidenkrantz Marit-Solveig [3], De Vernal Anne [4], Hu Bangqi [5], Song Bing [6], Jiang Hui [7, *], Sha Longbin [1, 2, 8, *]

[1] Donghai Academy, Ningbo University, Ningbo 315211, China
[2] Department of Geography and Spatial Information Techniques, Ningbo University, Ningbo 315211, China
[3] Department of Geoscience, Aarhus University, Aarhus 8000, Denmark
[4] Geotop-Université du Québec à Montréal, Montréal, QC H3C 3P8, Canada
[5] Laboratory for Marine Mineral Resources, Pilot National Laboratory for Marine Science and Technology, Qingdao 266061, China
[6] State Key Laboratory of Lake Science and Environment, Nanjing Institute of Geography and Limnology, Chinese Academy of Sciences, Nanjing 210008, China
[7] School of Geographic Sciences, East China Normal University, Shanghai 200062, China
[8] Laboratory for Marine Geology, Pilot National Laboratory for Marine Science and Technology, Qingdao 266061, China

* Corresponding authors : Hui Jiang, email address : hjiang@geo.ecnu.edu.cn ; Longbin Sha, email address : shalongbin@nbu.edu.cn

Abstract :

A reconstruction of sea-surface salinity (SSS) in the southern Okinawa Trough (OT) since 6800 cal. yr BP has been presented in this study. We found that the SSS record increased gradually from the middle to late Holocene, indicating reduced summer precipitation in Taiwan. Our results also suggest regional patterns of SSS with SSS increasing in the southern OT and decreasing in the northern OT since the mid-Holocene. Observational data indicate that the SSS in the southern and northern OT are strongly affected by fluvial discharge from Taiwan and the Changjiang River, linked to summer precipitation in South and Central Eastern China, respectively. The contrasting changes in SSS from the OT since the mid-Holocene suggest different spatial patterns of precipitation, with decreasing summer precipitation in South China and increasing summer precipitation in central-eastern China due to the weakened East Asian Summer Monsoon (EASM) and solar insolation. The delayed seasonal transitions of the EASM, with a longer Meiyu stage and a shorter midsummer stage from the mid-Holocene to late Holocene, are consistent with the delayed northward migration of the westerlies in the late Holocene.

Highlights

► Increasing SSS in the southern OT consistent with weakening EASM during the mid-Holocene. ► Regional patterns of SSS with differences between the southern and northern OT. ► Asynchronous summer precipitation patterns in southeastern and central eastern China. ► The regional EASM precipitation is indeed a determinant parameter of SSS for the OT.

Keywords : sea surface salinity, Okinawa Trough, precipitation, East Asian S ummer M onsoon

1. Introduction

As an important component of the global atmospheric circulation system, the East Asian Summer Monsoon (EASM) plays a significant role in global hydrological and energy cycles and is the primary driver of hydroclimatic changes in East Asia (An et al., 2015; Ding and Chan, 2005). Unlike other monsoons that have only one rainfall stage, the seasonal rainfall evolution over East Asia undergoes a number of quasi-stationary intraseasonal stages with abrupt transitions (Fig. S5). During spring, persistent rainfall in southern China is followed by substantial convection over the South China Sea during the pre-Meiyu stage in mid-May. By mid-June, the Meiyu begins and rainfall shifts to central China, and around mid-July, the rain band shifts again to be located over northeast China, marking the onset of the midsummer stage, which terminates around mid-August (Chiang et al., 2015). In recent decades, the variability of the EASM has been studied intensively using various archives. Speleothem $\delta^{18}O$ records, in particular, have been widely used for evaluating EASM intensity on various timescales due to their advantages of high precision uranium-series dating and high temporal resolution (An et al., 2015; Cheng et al., 2016; Dykoski et al., 2005; Liu et al., 2014; Wang et al., 2005; Yuan et al., 2004).

The East China Sea, a marginal sea in the northwestern Pacific, is characterised by

one of the largest continental shelves on Earth, where the EASM strongly influences surface waters (Chang et al., 2009; Kutoba et al., 2010; Sun et al., 2005). Sea surface salinity (SSS) is affected by atmospheric forcing (e.g. evaporation, precipitation, and wind), and fluvial runoff (Chen et al., 2006). SSS measurements obtained from the East China Sea during 1997–2001 indicate that river discharge, rather than precipitation over the ocean surface, is the main modulator of SSS in the East China Sea (Delcroix and Murtugudde, 2002).

The Okinawa Trough (OT) is a curved basin behind the Ryukyu Island Arc, constituting the southeastern part of the East China Sea, with a maximum water depth exceeding 2000 m (Fig. 1). Forming a passage between continental China and the northwestern Pacific Ocean, OT sediments are expected to provide a paleoenvironmental record of both continental and oceanic influences during the last deglaciation (Wang et al., 2016). Almost all the previous SSS reconstructions from the OT were based on estimates of the oxygen isotope composition of seawater ($\delta^{18}O_{sw}$) (Chang et al., 2009; Jian et al., 2000; Kubota et al., 2010; Lin et al., 2006; Sun et al., 2005; Wang et al., 2016; Xiang et al., 2007; Yu et al., 2009). However, additional reliable proxies of past SSS variability are required to improve our understanding of its long-term evolution.

Diatoms are widely used in Holocene palaeoceanography and palaeoclimatology because of their sensitivity and rapid response to environmental changes such as sea

surface temperature (SST) and SSS (Jiang et al., 2015; Zong et al., 2006; Shirota et al., 2021). Analyses of diatom assemblages from surface sediments of the western Pacific marginal seas suggest that summer SSS is one of the two main environmental factors controlling diatom distribution (Huang et al., 2012). Therefore, down-core diatom data from core MD05-2908 were used to reconstruct past variations in summer SSS in the southern OT during the mid- to late Holocene. Diatom assemblages and quantitative SSS estimates spanning the last 1000 years were presented by Li et al. (2012). Here, we extend the record back to 6800 years BP, focusing on diatom-based SSS reconstructions. A comparison with data from the study region led us to pinpoint regional differences in the impact of the EASM on precipitation in southern and northern East China.

2. Regional Setting

The southern OT has a typical subtropical monsoon climate, with hydrological conditions strongly influenced by air temperature, humidity, and atmospheric circulation (Fig. 1; Li et al., 2012). An important oceanographic feature of the OT is the Kuroshio Current, which originates from the northward branch of the North Equatorial Current and flows off the Philippine coast. The Kuroshio Current enters the OT in the East China Sea through the Yonaguni Depression, flows northeastward along the shelf slope of the East China Sea near the 200 m isobath, and exits to the open Pacific through the Tokara Strait. A coastal counter-current in I-Lan Bay, characterised by lower salinity and temperature than the main Kuroshio Current,

flows in the opposite direction off the north coast of Taiwan. This counter-current flows clockwise into the Keelung Sea Valley and I-Lan Bay before continuing southward across the I-Lan Shelf and turning northeastward, mixing with the Kuroshio Current, thus diluting the SSS. Although the countercurrents have been documented to occur in every season, their intensity is stronger in summer because of the southwesterly monsoon (Hsu et al., 2018).

The particulate load of rivers in Taiwan is a major source of detrital sediments to the southern OT. Because of high erosional gradients and heavy rainfall, Taiwan's rivers deliver 263 million tons (Mt) of sediment to the sea annually (191 Mt from western Taiwan and 72 Mt from eastern Taiwan) (Hsu et al., 2004). The annual total sediment yield of the Lanyang River in northeastern Taiwan is 6–9 Mt (Diekmann et al., 2008). During periods of high runoff, terrigenous sediments from the Lanyang River were rapidly transported to the southern OT. During the low runoff period, owing to weakened hydrodynamic flows, terrestrial sediments were temporarily deposited on the I-Lan Shelf and ridge. Subsequently, they can be resuspended and transferred to the OT by runoff from floods or occasionally from major earthquakes (Hsu et al., 2004; Huh et al., 2006). In addition, a portion of the sediment discharge from other eastern and western Taiwanese rivers is carried northward by currents (i.e. the Kuroshio Current off eastern Taiwan and the Taiwan Warm Current (TWC) in the Taiwan Strait) (Fig. 1; Hsu et al., 2004).

3. Data and methods

3.1 Diatom data and a diatom-based SSS transfer function

Diatom data were extracted from piston core MD05-2908 (24°48.04′N, 122°29.35′E; Fig. 1). This 34.16-m-long core was obtained from the southern OT at a water depth of 1276 m during the IMAGES XII cruise, 2005. Diatom samples were prepared following Håkansson (1984). More than 300 diatom valves were counted in random transects for each sample (excluding *Chaetoceros* resting spores). A total of 248 samples, each representing a 1-cm-thick slice of sediment, covering the last 6800 years, were analysed for their diatom contents. Li et al. (2015) published the diatom assemblage results of this core (Fig. S1), which were used for the reconstruction of summer SSS variability in this study with a high time resolution of ~27 years for the entire record.

The SSS was reconstructed using a diatom-based transfer function based on a revised modern calibration dataset of diatoms and environmental variables measured in the western Pacific marginal seas (Table S1, Fig. S2; Huang et al., 2009; Li et al., 2012). Seven numerical approaches were evaluated, and weighted averaging partial least squares (WA-PLS) with component 3 was employed to quantitatively reconstruct the SSS using the C2 software (cf. Table S2). Furthermore, plots of modern observed SSS *versus* estimated SSS based on diatom data from the same sample sites showed a good linear correlation, and the residuals were randomly scattered (Fig. S3).

3.2 Chronology

Seventeen accelerator mass spectrometry (AMS) ^{14}C ages were obtained from planktic foraminifera populations of *Globigerinoides ruber* and *G. sacculifer* (Table S3) at the AMS ^{14}C Dating Centre of the Woods Hole Oceanographic Institution. The ^{14}C ages were calibrated using the OxCal v. 4.4 program (Bronk Ramsey, 2009) with the Marine20 marine calibration curve (Heaton et al., 2020), applying a local marine reservoir age ($\triangle R$) of –109 ± 25 years (Hideshima et al., 2001). An age model was constructed based on the depositional model option in OxCal with a *k* value of 5 (Fig. S4).

3.3 Time series analysis

To detect the most important variations in summer SSS, we first performed ensemble empirical mode decomposition (EEMD; Huang and Wu, 2008), which is a noise-assisted data analysis of the reconstructed summer SSS. We calculated the power spectrum of the detrended summer SSS using the Morlet wavelet technique to determine its statistical significance (Schulz and Mudelsee, 2002).

3.4 Modern data

To identify the possible mechanisms of the regional SSS variations in the OT, we investigated the possible links between observed SSS, precipitation, and EASM intensity over the past 60 years. SSS data were obtained from the Ocean Reanalysis System 5 (ORAS5)

(https://www.ecmwf.int/en/forecasts/dataset/ocean-reanalysis-system-5), and precipitation data were extracted from the ERA5 dataset (https://www.ecmwf.int/en/forecasts/datasets/reanalysis-datasets/era5) produced by the European Centre for Medium-Range Weather 40 Forecasts (ECMWF). We used the EASM index of Li and Zeng (2002) to measure EASM intensity, which has been widely used in previous studies (Li and Zeng, 2002; Wu et al., 2016). This index was constructed as the dynamically normalised seasonality of the wind field, with the monsoon strength being the magnitude of the seasonal difference in the wind field. Index t is defined as follows:

$$\delta = \frac{\| \overline{V}_1 - \overline{V}_i \|}{\| \overline{V} \|} - 2$$

where $\overline{V}_1$, $\overline{V}_i$ are the January climatological and monthly wind vectors at a point, respectively, and $\overline{V}$ is the mean of the January and July climatological wind vectors at that point. Norm $\| A \|$ is defined as follows:

$$\|A\| = (\iint S|A|^2 \, dS)^{1/2}$$

where S denotes the domain of integration (10–40°N, 110–140°E). The monthly mean wind speed data at 850 hPa used to calculate the EASM index from 1958 to 2017 were obtained from the reanalysis datasets of the National Centre for Environmental Prediction–National Centre for Atmospheric Research (NCEP-NCAR) (https://psl.noaa.gov/data/gridded/data.ncep.reanalysis.html).

The correlation coefficients between the EASM index and SSS in the East China Sea,

and summer mean precipitation in the southern and central part of the larger East China Sea region were calculated pixel by pixel with the statistical package R. The global polynomial interpolation method in ArcGIS software was used to capture coarse-scale patterns in the correlation coefficients data with a 1° × 1° spatial resolution. The result from this tool is a smooth surface that represents gradual trends in the surface over the area of interest, as shown in Fig. 5A and 5B.

4. Results and discussion

4.1 Reconstructed SSS in the southern OT and comparison with other records from adjacent areas

The reconstructed SSS of the southern OT ranges between 33.1 and 34.1 psu and shows a generally increasing trend over the past 6800 years (Fig. 2A). The modern SSS in summer (June-July-August, JJA) near site MD05-2908 was 33.95 psu (Japan Oceanographic Data Center (JODC), J-DOSS, 1 Degree Gridded Salinity Statistics, 1906–2003, available at http://www.jodc.go.jp/index_j.html). Superimposed on the increasing salinity trend are shorter-term variations ranging in length from millennia to decades. The SSS was well below the mean value (33.6 psu) from 6800 to 4000 cal. yr BP, although this lower salinity interval was interrupted by an interval of relatively high SSS from 6600–6000 cal. yr BP (Fig. 2A). The relative abundance of coastal-water diatoms (the sum of diatom valves belonging to the genus *Cyclotella*, *Diponeis* and *Paralia*) in core MD05-2908 shows high values from 6800 to 4000 cal. yr BP while our reconstructions indicate low SSS (Fig. 4A; Fig. S1; Li et al., 2015).

Shirota et al. (2021) also used the abundance of coastal water diatoms *Paralia* spp. in the northern OT to assess on the expansion of coastal water during the LGM to early deglaciation, which may contribute to lower SSS.

After ca. 4000 cal. yr. BP, the SSS increased rapidly until ~3300 cal. yr BP, albeit with an interval of exceptionally low SSS centred at approximately 3600 cal. yr BP. The SSSs were generally above the mean value for the record after 3300 cal. yr BP, with two periods of the highest SSS during 3000–2400 cal. yr BP and after 1000 cal. yr BP (Fig. 2A). The increase in SSS after 4000 cal. yr BP corresponds with a remarkable decrease in the abundance of coastal water diatoms (Fig. 4A). The correlation coefficient between the coastal water diatoms and the SSS is -0.76 ($p<0.01$) over the last 6800 years, indicating that changes in coastal water fluxes, as indicated by coastal water diatoms, play a key role in the SSS in the southern OT.

To detect the dominant oscillations in the SSS over the past 6800 years, we used variations in the EEMD components (c1–c8), shown in Fig. 3A. Considering the duration and temporal resolution of the reconstructed SSS record, we removed the long-term trend and decadal-scale noise, and selected the sum of c2–6 (c2+c3+c4+c5+c6) to reproduce the information recorded in the SSS, which also exhibited oscillations. To detect the specific periods of the dominant components, we performed a spectral analysis of the detrended SSS (sum c2–6). The results revealed the following significant periodicities (above the 95% confidence level): 372 yr, 212

yr, 150 yr, 124 yr, 110 yr and 90 yr (Fig. 3B and 3C). Among them, the 212-yr, 124-yr, 110-yr and 90-yr periodicities in the reconstructed SSS record are similar to those of EASM intensity during the Holocene as revealed by the stalagmite $\delta^{18}O$ record from Dongge Cave (periodicities of 217 yr, 127 yr, 109 yr and 85 yr) (Dykoski et al., 2005). The 212-yr and 90-yr periodicities were close to those of the de Vries (~208 y) and Gleissberg (~88 y) solar cycles (Steinhilber et al., 2012). Therefore, changes in SSS in the southern OT follow the oscillations of the EASM, which are often attributed to variations in solar activity. Decreasing solar insolation over the last 6800 years may have been the driver of the continuously decreasing EASM (Fig. 2B). During the mid-Holocene, solar insolation was relatively high, resulting in an enhanced EASM and warm climate, while decreased solar insolation in the late Holocene led to a weakened EASM and cool climate.

To further evaluate the relationship between SSS in the southern OT and the EASM, running correlation coefficients of SSS versus stalagmite $\delta^{18}O$ values from Dongge Cave, a proxy for past EASM intensity (Fig. 2B; Dykoski et al., 2005), were calculated for selected sliding windows, which includes a random phase test that takes into account the autocorrelations of the time series (Fig. 2C). The results indicate a robust positive correlation between SSS and the stalagmite $\delta^{18}O$ records during the mid- to late Holocene, except after 1500 cal. yr BP (Fig. 2C). The most negative stalagmite $\delta^{18}O$ values at Dongge Cave indicate the maximum strength of the EASM from ~8000 to 6000 cal. yr BP, followed by a decrease (Dykoski et al., 2005; Wang et

al., 2005). The trend of increasing SSS in the southern OT as reconstructed based on our diatom record (Fig. 4A) and based on the $\delta^{18}O_w$ record from core OKT-3 (Fig. 4B; Wang et al., 2016), is consistent with the weakening of EASM deduced from the stalagmite $\delta^{18}O$ records in both South and North China, in phase with weakening summer insolation in the Northern Hemisphere during the Holocene (Dykoski et al., 2005; Wang et al., 2005; Yang et al., 2019). However, the $\delta^{18}O_w$-based SSS at sites A7 and MD012404 in the middle OT show no significant trend during the mid- to late Holocene (Fig. 4C and 4D; Chen et al., 2010; Sun et al., 2005). On the contrary, the $\delta^{18}O_w$ from core KY07-04-01 suggests a slight decreasing trend of SSS since the mid-Holocene (Fig. 4E; Kubota et al., 2010). These results suggest that SSS variations may show regional patterns with contrasts between the southern and northern OT, with SSS increasing in the southern OT and decreasing in the northern OT when the EASM weakened during the mid- to late Holocene.

4.2 Possible mechanism

To identify the possible mechanisms of regional SSS variations in the OT, we correlated the modern SSS for the OT with the EASM index for 1958–2017 (Fig. 5A). This result is in general agreement with our proxy records, showing a negative correlation between summer SSS and the EASM index in the southern OT but positive correlations between summer SSS and the EASM index in northern OT. This shows that regionalism in the southern and northern OT was also observed in modern instrumental data.

We further correlated the EASM index with the observed summer precipitation in southeastern China, central-eastern China, and adjacent areas (Fig. 5B). The results revealed a positive correlation between the EASM index and summer precipitation in southeastern China, Taiwan, and the southern OT, but a negative correlation in central-eastern China and the northern OT (Fig. 5B). This suggests an antiphase in rainfall from southeastern and central-eastern China.

Previous studies have demonstrated that the modern summer precipitation over East Asia shows a meridional "tripole" pattern, with summer precipitation increasing in central-eastern China (including the Changjiang Basin) but decreasing in southeastern/northeastern China during periods of weakened EASM, and *vice versa* (Fig. S5; Hsu and Lin, 2007; Wu et al., 2016). Modern SSS changes in the East China Sea are likely due to anomalous river discharge, and hence, an integration of precipitation anomalies over large continental areas (Delcroix and Murtugudde, 2002). In particular, the SSS in the northern part of the East China Sea is mainly controlled by changes in the discharge of the Changjiang River (also called the Yangtze River) during summer and the hydrodynamic conditions of the Changjiang River catchment (Kitani, 1998), which may be detectable in the northern OT (Kubota et al., 2015). Furthermore, based on a study of the flooding of the Changjiang River in the summer of 2010, which was the highest magnitude of flooding over the past decades, Chen et al. (2015) found that low SSS covered almost two-thirds of the continental shelf

because of the extremely large volumes of freshwater delivered to the East China Sea. Despite this extreme situation, the impact of the Changjiang River discharge on SSS distribution did not influence the southern OT region.

Therefore, as changes in the EASM and precipitation affect the amount of freshwater delivered to the OT through river systems, it is not surprising that summer SSS variations broadly follow changes in regional summer precipitation. High summer precipitation in central-eastern China intensified freshwater discharge from the Changjiang River in the northern OT during a period of weak EASM, leading to a decrease in SSS in the northern OT (Fig. 5). In contrast, summer precipitation over southeastern China and Taiwan decreased when the EASM weakened, resulting in decreased fluvial discharge and increased SSS in the southern OT (Fig. 5). The regionalism in SSS variations in the southern and northern OT can thus be related to the asynchronous summer precipitation patterns in southeastern and central-eastern China.

The antiphase relationship proposed above probably applies to palaeohydroclimatic variations. The stalagmite $\delta^{18}O$ record from Dongge Cave (Dykoski et al., 2005; Wang et al., 2005) and Sanbao Cave (Dong et al., 2010), and a stacked synthesised $\delta^{18}O$ record from China (Yang et al., 2019), indicate a general weakening of the EASM intensity during the Holocene (Fig. 6A-C). Moreover, a record from Retreat Lake in Taiwan suggests a weaker EASM since the mid-Holocene (Selvaraj et al.,

2011). Numerous studies have shown that the dominant mode of summer rainfall variability over East Asia at long timescales is also characterised by an out-of-phase pattern between southeastern and central-eastern China (Chiang et al., 2017; Hsu, 2003; Zhang et al., 2018). A transient simulation study of the Holocene revealed that southeastern and southwestern China recorded higher precipitation during the early to mid-Holocene than today, whereas central-eastern China received less precipitation (Jin et al., 2014).

Some moisture indices (e.g. pollen- and pollen-based proxies from South China and a precipitation record from the Pearl River Estuary) indicate humid conditions during the mid-Holocene (~7000–4000 cal. yr BP), and a dryer climate during the past ~4000 years in southeastern China (Fig. 6D–E; Ran and Feng, 2013; Strong et al., 2013). The tree pollen percentages, which were used as moisture proxies, suggest a persistently humid climate from ~11000 to ~5000 cal. yr BP in Erhai Lake in southwestern China, followed by a drier climate (Dearing et al., 2008). Furthermore, pollen records from Huguangyan Maar Lake indicate moderately humid conditions between ~7800 and ~4200 cal. yr BP and a dry phase since ~4200 cal. yr BP (Fig. 6G; Wang et al., 2007). This is further supported by Huang et al. (2020), who used a moisture index based on pollen and charcoal concentrations in the Toushe Basin in central Taiwan, which indicated a warm and humid climate from 6200 to 4600 cal. yr BP and dry climatic conditions from 3700 to 2000 cal. yr BP (Fig. 6F).

The increasing mid-Holocene to late Holocene trend in the SSS in the southern OT may be related to a decrease in summer precipitation over southeastern China and Taiwan since 6800 cal. yr BP. Regional summer precipitation is a determining parameter of modern SSS in the region. The spatial distribution of modern particle fluxes suggests that the terrestrial input to the southern OT is mainly derived from Taiwan Island and mainland China, including delivery by the coastal current off East China and the resuspension of sediments from the continental shelf (Huh et al., 2006; Kao et al., 2003). However, by measuring sediment fluxes, Hsu et al. (2004) found that sediments from eastern Taiwan were the dominant source of supply to the southern OT. Geochemical records from the southern OT show that the Holocene depositional environment was controlled by the activity of the complex Kuroshio Current system, which carries the sediment load of the Lanyang River (northeastern Taiwan) from the I-Lan Ridge to the southern OT (Diekmann et al., 2008; Dou et al., 2016). On seasonal and interannual scales, the axis of the Kuroshio Current shifts seaward northeast of Taiwan in summer and shoreward in winter because of monsoon forcing (Ma et al., 2009; Tang, 2000). This results in a weaker impact of freshwater discharge in the study area in summer than in winter. However, on a millennial scale, there has been no significant change in the abundance of diatom species related to the Kuroshio Current since the mid-Holocene (Li et al., 2015); thus, the strength of the Kuroshio Current was probably stable since ~7300 cal. yr BP, when the main flow re-entered the OT (Jian et al., 2000). When the influence of the coastal waters off northeastern Taiwan was strong, the SSS in the southern OT tended to be less saline,

and *vice versa*. Thus, the gradual increase in the SSS in the southern OT may have mostly resulted from the weakening of the coastal waters off northeastern Taiwan (Chen et al., 2015; Dykoski et al., 2005; Hsu et al., 2018), which further reduced the impact of decreasing regional precipitation over the past 6800 years.

Summer precipitation in the Changjiang River Valley in central China has experienced a different spatial pattern since the mid-Holocene. The precipitation proxy records from the Dajiuhu peatland (31°29′ N, 110°00′ E) and a stalagmite from Heshang Cave (30°27′ N, 110°25′ E) in central eastern China (32–28°N, 103–122°E), show relatively dry conditions during the 7000–3000 cal. yr BP and wetter conditions after 3000 cal. yr BP, which agrees with the timing of several documented flooding and aridification events in central-eastern China (Fig. 6H; Liu et al., 2020; Xie et al., 2013; Zhu et al., 2017). A prominent mid-Holocene drought is further evidenced by the environmental magnetic parameters of the speleothem $IRM_{soft\text{-}flux}$ from Heshang Cave (Zhu et al., 2017), and the depth of the water table reconstructed based on phytoliths (Liu et al., 2019) from the Dajiuhu peatland. Extreme palaeofloods were also more frequent in central China after 2200 cal. yr BP (Zhu et al., 1997). In addition, the simulated precipitation over the East Asian monsoon region showed a slight increasing trend in central-eastern China during the late Holocene (Fig. 6I; Dallmeyer et al., 2015). According to modern observations, summer SSS variations in northern OT are mainly controlled by the Changjiang River discharge (Kubota et al., 2015), which reflects summer precipitation in central-eastern China (Fig. 5).

Therefore, increased summer precipitation in central-eastern China during Holocene resulted in increased freshwater discharge from the Changjiang River and, subsequently, an increased dilution effect on the northern OT, leading to a decrease in SSS in the region (Kubota et al., 2010). Previous studies have also shown that the influence of the Changjiang River was strong in the northern OT but weak in the southern OT after ~9200 cal. yr BP (Lie et al., 2003; Wang et al., 2016). This evidence indicates that different summer precipitation patterns characterise southeastern China, Taiwan, and central-eastern China (Jia et al., 2015; Li et al., 2014; Lu et al., 2013). Hence, SSS signatures may have differed substantially from one region to another between the southern OT (Wang et al., 2016) and northern OT (Kubota et al., 2010; Sun et al., 2005) during the Holocene.

According to Chiang et al. (2015), Meiyu began in mid-June, and rainfall shifted to central-eastern China; by mid-July, the rain band shifted again to a location over northeastern China, marking the onset of the mid-summer stage, which terminated around mid-August (Fig. S5). On longer timescales, the early to mid-Holocene was characterised by a shorter Meiyu stage and a longer midsummer stage, leading to less rain over central-eastern China and more rain over southeastern China, compared to the late Holocene, as suggested by palaeoclimate modelling studies (Kong et al., 2017; Zhang et al., 2018). This suggests the occurrence of increased summer precipitation over southeastern China and reduced precipitation over central-eastern China in the mid-Holocene compared with the late Holocene (Chiang et al., 2015; Zhang et al.,

2018). Therefore, the decrease in summer precipitation in southeastern China and Taiwan inferred from the increasing SSS in the southern OT since the mid-Holocene was likely associated with a longer Meiyu stage and a shorter midsummer stage over East China caused by a lag in the onset of the Meiyu and midsummer stages (Kong et al., 2017). Chiang et al. (2015) and Kong et al. (2017) explained earlier seasonal transitions (a shorter Meiyu stage and a longer midsummer stage) in the EASM during the mid-Holocene as northward transitions of the westerlies relative to the Tibetan Plateau due to a reduced meridional insolation gradient (Zhang et al., 2018). Therefore, during the late Holocene, a longer Meiyu stage and a shortened midsummer stage (Kong et al., 2017), which resulted in a decrease in EASM precipitation in southeastern China and Taiwan, were likely due to the southward shift of the westerlies, consistent with delayed northward migration. Such delayed migration could be linked to colder conditions in the northern extratropics and the slowdown of the Atlantic Meridional Overturning Circulation (AMOC), which intensifies the equator-to-pole temperature gradient (Zhang et al., 2018). However, summer precipitation in the Changjiang River valley in central-eastern China has experienced a different spatial pattern since the mid-Holocene.

5. Conclusion

We present a diatom-based SSS record from the southern OT, spanning the past 6800 years. The reconstructed SSS showed an increasing trend from the mid-Holocene to the present, suggesting a decrease in summer precipitation over Taiwan. This trend is

consistent with other records from South China but differs from the pattern of increased summer precipitation in central-eastern China.

Our reconstruction also suggests regional patterns of SSS with differences between the southern and northern OT. Investigation of the underlying mechanisms indicated that SSS in the southern and northern OT was strongly affected by fluvial discharge from Taiwan and the Changjiang River, linked to summer precipitation in South and central-eastern China, respectively. Observational data also indicate increased precipitation over South China and reduced precipitation over central-eastern China during a strong EASM. We attribute the contrasting variations in SSS in the southern and northern OT since the mid-Holocene to different spatial patterns of precipitation, with decreasing summer precipitation in South China and increasing summer precipitation in central-eastern China due to the weakened EASM and solar insolation. The different patterns between South and central-eastern China can also be attributed to the delayed seasonal transitions of the EASM, with a longer Meiyu stage and a shorter mid-summer stage from the middle to late Holocene, which is consistent with the delayed northward migration of the westerlies in the late Holocene.

Acknowledgments:

We are grateful to the Institute Paul-Emil Victor for the Marco Polo 2 IMAGES coring operation onboard the R/V *Marion Dufresne* in 2005, and to the captain and crew. We sincerely thank Prof. Tiegang Li of the First Institute of Oceanography,

MNR, China, for providing the sediment samples. This work was supported by the National Natural Science Foundation of China (Nos. 42376236, 42176226 and 41876215) and the Fundamental Research Funds for the Provincial Universities of Zhejiang (No. SJLY2020004). We thank Dr. Jan Bloemendal for suggesting improvements to the English text.

References

An, Z., Wu, G., Li, J., Sun, Y., Liu, Y., Zhou, W., et al., 2015. Global monsoon dynamics and climate change. Annu. Rev. Earth Planet. Sci. 43, 29-77. https://doi.org/10.1146/annurev-earth-060313-054623.

Bronk Ramsey, C., 2009. Bayesian analysis of radiocarbon dates. Radiocarbon 51, 337-360. https://doi.org/10.1017/S0033822200033865.

Chang, Y.-P., Chen, M.-T., Yokoyama, Y., Matsuzaki, H., Thompson, W.G., Kao, S.-J., Kawahata, H., 2009. Monsoon hydrography and productivity changes in the East China Sea during the past 100,000 years: Okinawa Trough evidence (MD012404). Paleoceanography 24, PA3208. https://doi.org/10.1029/2007PA001577.

Chen, X.Y., Wang, X.H., Guo, J.S., 2006. Seasonal variability of the sea surface salinity in the East China Sea during 1990–2002. J. Geophys. Res. 111, C05008. https://doi.org/10.1029/2005JC003078.

Chen, C.-C., Gong, G.-C., Chou, W.-C., Chung, C.-C., Shiah, F.-K., Chiang, K.-P. Effects of flooding on organic carbon consumption in the East China Sea, Biogeosciences Discuss., 12, 5609–5639, https://doi.org/10.5194/bgd-12-5609-2015, 2015.

Chen, M.T., Lin, X.P., Chang, Y.P., Chen, Y.C., Lo, L., Shen, C.C., Yokoyama, Y., Oppo, D.W., Thompson, W.G., Zhang, R., 2010. Dynamic millennial-scale climate changes in the northwestern Pacific over the past 40,000 years. Geophys. Res. Lett. 37, L23603. https://doi.org/10.1029/2010GL045202.

Cheng, H., Edwards, R.L., Sinha, A., Spotl, C., Yi, L., Chen, S., Kelly, M., Kathayat, G., Wang, X., Li, X., Kong, X., Wang, Y., Ning, Y., Zhang, H., 2016. The Asian monsoon over the past 640,000 years and ice age terminations. Nature 534, 640–646. https://doi.org/10.1038/nature18591.

Chiang, J.C.H., Fung, I.Y., Wu, C.-H., Cai, Y., Edman, J.P., Liu, Y., Day, J.A., Bhattacharya, T., Mondal, Y., Labrousse, C.A., 2015. Role of seasonal transitions and westerly jets in East Asian paleoclimate. Quat. Sci. Rev. 108, 111–129. https://doi.org/10.1016/j.quascirev.2014.11.009.

Chiang, J.C.H., Swenson, L.M., Kong, W., 2017. Role of Seasonal Transitions and the Westerlies in the Interannual Variability of the East Asian Summer Monsoon Precipitation. Geophys. Res. Lett. 44, 3788–3795. https://doi.org/10.1002/2017GL072739.

Dallmeyer, A., Claussen, M., Fischer, N., Haberkorn, K., Wagner, S., Pfeiffer, M., Jin, L., Khon, V., Wang, Y., Herzschuh, U., 2015. The evolution of sub-monsoon systems in the Afro-Asian monsoon region during the Holocene– comparison of different transient climate model simulations. Clim. Past. 11, 305–326. https://doi.org/10.5194/cp-11-305-2015.

Dearing, J.A., Jones, R.T., Shen, J., Yang, X., Boyle, J.F., Foster, G.C., Crook, D.S., Elvin, M.J., 2008. Using multiple archives to understand past and present climate–human–environment interactions: the lake Erhai catchment, Yunnan Province, China. J. Paleolimnol. 40, 3-31. https://doi.org/10.1007/s10933-007-9182-2.

Delcroix, T., Murtugudde, R., 2002. Sea surface salinity changes in the East China Sea during 1997-2001: Influence of the Yangtze River. J. Geophys. Res. 107, SRF 9-1-SRF 9–11. https://doi.org/10.1029/2001JC000893.

Diekmann, B., Hofmann, J., Henrich, R., Fütterer, D.K., Röhl, U., Wei, K.-Y., 2008. Detrital sediment supply in the southern Okinawa Trough and its relation to sea-level and Kuroshio dynamics during the late Quaternary. Mar. Geol. 255, 83–95. https://doi.org/10.1016/j.margeo.2008.08.001.

Ding, Y.H., Chan, J.C.L., 2005. The East Asian summer monsoon: an overview. Meteorog. Atmos. Phys. 89, 117–142. https://doi.org/10.1007/s00703-005-0125-z.

Dong, J.G., Wang, Y.J., Cheng, H., Hardt, B., Edwards, R.L., Kong, X., et al., 2010. A high-resolution stalagmite record of the Holocene East Asian monsoon from Mt Shennongjia, central China. Holocene, 20(2), 257–264. https://doi.org/10.1177/0959683609350393.

Dou, Y.G., Yang, S.Y., Shi, X.F., Clift, P.D., Liu, S.F., Liu, J.H., Li, C., Bi, L., Zhao, Y., 2016. Provenance weathering and erosion records in southern Okinawa Trough sediments since 28 ka: geochemical and Sr-Nd-Pb isotopic evidences. Chem. Geol. 425, 93–109. https://doi.org/10.1016/j.chemgeo.2016.01.029.

Dykoski, C.A., Edwards, R.L., Cheng, H., Yuan, D., Cai, Y., Zhang, M., Lin, Y., Qing, J., An, Z., Revenaugh, J., 2005. A high-resolution, absolute-dated Holocene and deglacial Asian monsoon record from Dongge Cave, China. Earth. Planet. Sci. Lett 233, 71-86. https://doi.org/10.1016/j.epsl.2005.01.036.

Heaton, T.J., Köhler, P., Butzin, M., Bard, E., Reimer, R.W., Austin, W.E.N., Bronk Ramsey, C., Grootes, P.M., Hughen, K.A., Kromer, B., Reimer, P.J., Adkins, J., Burke, A., Cook, M.S., Olsen, J., Skinner, L.C., 2020. Marine20—The Marine Radiocarbon Age Calibration Curve (0–55,000 cal BP). Radiocarbon 62, 779–820. https://doi.org/10.1017/RDC.2020.68.

Hideshima, S., Matsumoto, E., Abe, O., Kitagawa, H., 2001. Northwest Pacific Marine Reservoir Correction Estimated from Annually Banded Coral from Ishigaki Island, Southern Japan. Radiocarbon 43(2A), 473–476. https://doi.org/10.1017/S0033822200038352.

Hsu, H.-H., 2003. Relationship between the Tibetan Plateau heating and East Asian summer monsoon rainfall. Geophys. Res. Lett. 30, 30–33. http://doi.org/10.1029/2003GL017909.

Hsu, S., Lin, F., Jeng, W., Chung, Y., Shaw, L., Hung, K., 2004. Observed sediment fluxes in the southwesternmost Okinawa Trough enhanced by episodic events: flood runoff from Taiwan rivers and large earthquakes. Deep-Sea Res. I 51, 979-997. https://doi.org/10.1016/j.dsr.2004.01.009.

Hsu, H.-H., Lin, S.-M., 2007. Asymmetry of the Tripole Rainfall Pattern during the East Asian Summer. J. Clim. 20, 4443–4458. https://doi.org/10.1175/JCLI4246.1.

Hsu, P.-C., Zheng, Q., Lu, C.-Y., Cheng, K.-H., Lee, H.-J., Ho, C.-R., 2018. Interaction of coastal countercurrent in I-Lan Bay with the Kuroshio northeast of Taiwan. Cont. Shelf. Res. 171, 30–41. https://doi.org/10.1016/j.csr.2018.10.012.

Huh, C.A., Su, C.C., Wang, C.H., Lee, S.Y., Lin, I.T., 2006. Sedimentation in the Southern Okinawa Trough—rates, turbidites and a sediment budget. Mar. Geol. 231, 129–139. https://doi.org/10.1016/j.margeo.2006.05.009.

Huang, Y., Jiang, H., Björck, S., Li, T., Lu, H., Ran, L., 2009. Surface sediment diatoms from the western Pacific marginal seas and their correlation to environmental variables. Chin. J. Oceanol. Limnol., 27, 674–682. https://doi.org/10.1007/s00343-009-9211-2.

Huang, Z., Ma, C., Chyi, S.J., Tang, L., Zhao, L., 2020. Paleofire, Vegetation, and Climate Reconstructions of the Middle to Late Holocene From Lacustrine Sediments

of the Toushe Basin, Taiwan. Geophys. Res. Lett. 47, e2020GL090401. https://doi.org/10.1029/2020GL090401.

Huang, N.E., and Wu, Z.H., 2008. A review on Hilbert-Huang transform: method and its applications to geophysical studies. Rev. Geophys. 46, RG2006. https://doi.org/10.1029/2007RG000228.

Jia, G., Bai, Y., Yang, X., Xie, L., Wei, G., Ouyang, T., Chu, G., Liu, Z., Peng, P.A., 2015. Biogeochemical evidence of Holocene East Asian summer and winter monsoon variability from a tropical maar lake in southern China. Quat. Sci. Rev. 111, 51–61. https://doi.org/10.1016/j.quascirev.2015.01.002.

Jian, Z., Wang, P., Saito, Y., Wang, J., Pflaumann, U., Oba, T., Cheng, X., 2000. Holocene variability of the Kuroshio Current in the Okinawa Trough, northwestern Pacific Ocean. Earth. Planet. Sci. Lett 184, 305–319. https://doi.org/10.1016/S0012-821X(00)00321-6.

Jiang, H., Muscheler, R., Björck, S., Seidenkrantz, M.-S., Olsen, J., Sha, L.B., Sjolte, J., Eiríksson, J., Ran, L.H., Knudsen, K.-L., Knudsen, M. F., 2015. Solar forcing of Holocene summer sea-surface temperatures in the northern North Atlantic. Geology, 43(3), 203–206. https://doi.org/10.1130/G36377.1

Jin, L., Schneider, B., Park, W., Latif, M., Khon, V., Zhang, X., 2014. The spatial–temporal patterns of Asian summer monsoon precipitation in response to Holocene insolation change: a model-data synthesis. Quat. Sci. Rev. 85, 47–62. https://doi.org/10.1016/j.quascirev.2013.11.004.

Kao, S.J., Lin, F.J., Liu, K.K., 2003. Organic carbon and nitrogen contents and their isotopic compositions in surficial sediments from the East China Sea shelf and the southern Okinawa Trough. Deep-Sea Res. II 50, 1203–1217. https://doi.org/10.1016/S0967-0645(03)00018-3.

Kitani, K., 1998. Low salinity anomaly observed in the East China Sea by research vessel Yoko-maru (in Japanese), Newsl. 95, pp. 9–11, Seikai Natl. Fisheries Res. Inst., Fisheries Res. Agency, Nagasaki, Japan. (Available at http://snf.fra.affrc.go.jp/.) https://doi.org/10.1029/2009PA001891.

Kong, W., Swenson, L.M., Chiang, J.C.H., 2017. Seasonal Transitions and the Westerly Jet in the Holocene East Asian Summer Monsoon. J Clim. 30, 3343–3365. https://doi.org/10.1175/JCLI-D-16-0087.1.

Kubota, Y., Kimoto, K., Tada, R., Oda, H., Yokoyama, Y., Matsuzaki, H., 2010. Variations of East Asian summer monsoon since the last deglaciation based on Mg/Ca and oxygen isotope of planktic foraminifera in the northern East China Sea.

Paleoceanography 25, PA4205. https://doi.org/10.1029/2009PA001891.

Kubota, Y., Tada, R., Kimoto, K., 2015. Changes in East Asian summer monsoon precipitation during the Holocene deduced from a freshwater flux reconstruction of the Changjiang (Yangtze River) based on the oxygen isotope mass balance in the northern East China Sea. Clim. Past. 11, 265–281. https://doi.org/10.5194/cp-11-265-2015.

Li, D., Knudsen, M.F., Jiang, H., Olsen, J., Zhao, M., Li, T., Knudsen, K.L., Seidenkrantz, M.-S., Sha, L., 2012. A diatom-based reconstruction of summer sea-surface salinity in the Southern Okinawa Trough, East China Sea, over the last millennium. J. Quat. Sci. 27, 771–779. https://doi.org/10.1002/jqs.2562.

Li, D.L., Jiang, H., Knudsen, K.L., Björck, S., Olsen, J., Zhao, M.X., Li, T.G., Li, J.L., 2015. A diatom record of mid- to late Holocene palaeoenvironmental changes in the southern Okinawa Trough. J. Quat. Sci. 30, 32–43. https://doi.org/10.1002/jqs.2756.

Li, J., Zeng, Q., 2002. A unified monsoon index. Geophys. Res. Lett. 29(8), 1274. https://doi.org/10.1029/2001GL013874.

Li, Q., Wu, H.B., Guo, Z.T., Yu, Y.Y., Ge, J.Y., Wu, J.Y., Zhao, D.A., Sun, A.Z., 2014. Distribution and vegetation reconstruction of the deserts of northern China during the mid-Holocene. Geophys. Res. Lett. 41, 5184–5191. https://doi.org/10.1002/2014GL059952.

Lie, H.-J., Cho, C.-H., Lee, J.-H., Lee, S., 2003. Structure and eastward extension of the Changjiang River plume in the East China Sea. J. Geophys. Res. 108, C33077. https://doi.org/10.1029/2001JC001194.

Lin, Y.-S., Wei, K.-Y., Lin, I.-T., Yu, P.-S., Chiang, H.-W., Chen, C.-Y., Shen, C.-C., Mii, H.-S., Chen, Y.-G., 2006. The Holocene Pulleniatina Minimum Event revisited: Geochemical and faunal evidence from the Okinawa Trough and upper reaches of the Kuroshio current. Mar. Micropaleontol. 59, 153–170. https://doi.org/10.1016/j.marmicro.2006.02.003.

Liu, H., Gu, Y., Huang, X., Yu, Z., Xie, S., Cheng, S., 2019. A 13,000-year peatland palaeohydrological response to the ENSO-related Asian monsoon precipitation changes in the middle Yangtze Valley. Quat. Sci. Rev. 212, 80–91. https://doi.org/10.1016/j.quascirev.2019.03.034.

Liu, X.K., Liu, J.B., Chen, S.Q., Chen, J.H., Zhang, X., Yan, J.J., Chen, F.H., 2020. New insights on Chinese cave δ18O records and their paleoclimatic significance. Earth Sci. Rev. 207, 103216. https://doi.org/10.1016/j.earscirev.2020.103216.

Liu, Z., Wen, X., Brady, E.C., Otto-Bliesner, B., Yu, G., Lu, H., Cheng, H., Wang, Y., Zheng, W., Ding, Y., Edwards, R.L., Cheng, J., Liu, W., Yang, H., 2014. Chinese cave records and the East Asia Summer Monsoon. Quat. Sci. Rev. 83, 115–128. https://doi.org/10.1016/j.quascirev.2013.10.021.

Locarnini, R.A., Mishonov, A.V., Baranova, O.K., Boyer, T.P., Zweng, M.M., Garcia, H.E., Reagan, J.R., Seidov, D., Weathers, K., Paver, C.R., Smolyar, I., 2018. World Ocean Atlas 2018, Volume 1: Temperature. A. Mishonov Technical Ed.; NOAA Atlas NESDIS 81, 52 pp

Lu, H., Yi, S., Liu, Z., Mason, J.A., Jiang, D., Cheng, J., Stevens, T., Xu, Z., Zhang, E., Jin, L., Zhang, Z., Guo, Z., Wang, Y., Otto-Bliesner, B., 2013. Variation of East Asian monsoon precipitation during the past 21 k.y. and potential CO_2 forcing. Geology 41, 1023–1026. https://doi.org/10.1130/G34488.1.

Ma, C., Wu, D., Lin, X., 2009. Variability of surface velocity in the Kuroshio Current and adjacent waters derived from Argos drifter buoys and satellite altimeter data. Chinese Journal of Oceanology and Limnology 27, 208–217. http://dx.doi.org/10.1007/s00343-009-9260-6.

Peristykh, A. N., and P. E. Damon, 2003. Persistence of the Gleissberg 88-year solar cycle over the last ~12,000 years: Evidence from cosmogenic isotopes. J. Geophys. Res. 108(A1), SSH 1-1-SSH 1-15. https://doi.org/10.1029/2002JA009390.

Ran, M., Feng, Z., 2013. Holocene moisture variations across China and driving mechanisms: A synthesis of climatic records. Quatern. Int. 313–314, 179–193. https://doi.org/10.1016/j.quaint.2013.09.034.

Shirota, K., Okazaki, Y., Konno, S., Miyairi, Y., Yokoyama, Y., Kubota, Y., 2021. Changes in surface water masses in the northern East China Sea since the Last Glacial Maximum based on diatom assemblages. Prog. Earth Planet. Sci. 8, 66. https://doi.org/10.1186/s40645-021-00456-1.

Schulz, M., Mudelsee, M., 2002. REDFIT: Estimating red-noise spectra directly from unevenly spaced paleoclimatic time series. Comput. Geosci-uk. 28, 421–426. https://doi.org/10.1016/S0098-3004(01)00044-9.

Selvaraj, K., Chen, C.T.A., Lou, J.Y., Kotlia, B., 2011. Holocene weak summer East Asian monsoon intervals in Taiwan and plausible mechanisms. Quatern. Int. 229(1-2), 57–66. https://doi.org/10.1016/j.quaint.2010.01.015.

Steinhilber, F., Abreu, J. A., Beer, J., Brunner, I., Christl, M., Fischer, H., 2012. 9,400 years of cosmic radiation and solar activity from ice cores and tree rings. PNAS 109, 5967–5971. https://doi.org/10.1073/pnas.1118965109.

Strong, D., Flecker, R., Valdes, P.J., Wilkinson, I.P., Rees, J.G., Michaelides, K., Zong, Y.Q., Lloyd, J.M., Yu, F.L., Pancost, R.D.J., 2013. A new regional, mid-Holocene palaeoprecipitation signal of the Asian Summer Monsoon. Quat. Sci. Rev. 78, 65–76. https://doi.org/10.1016/j.quascirev.2013.07.034.

Sun, D., Gagan, M.K., Cheng, H., Scott-Gagan, H., Dykoski, C.A., Edwards, R.L., Su, R., 2005a. Seasonal and interannual variability of the Mid-Holocene East Asian monsoon in coral $\delta^{18}O$ records from the South China Sea. Earth. Planet. Sci. Lett 237, 69–84. https://doi.org/10.1016/j.epsl.2005.06.022.

Sun, Y., Oppo, D.W., Xiang, R., Liu, W., Gao, S., 2005b. Last deglaciation in the Okinawa Trough: Subtropical northwest Pacific link to Northern Hemisphere and tropical climate. Paleoceanography 20. https://doi.org/10.1029/2004PA001061.

Tang, T., 2000. The flow pattern north of Taiwan and the migration of the Kuroshio. Cont. Shelf. Res. 20, 349–371. https://doi.org/10.1016/S0278-4343(99)00076-X.

Wang, L., Li, J., Zhao, J., Wei, H., Hu, B., Dou, Y., Sun, Z., Zou, L., Bai, F., 2016. Solar-, monsoon- and Kuroshio-influenced thermocline depth and sea surface salinity in the southern Okinawa Trough during the past 17,300 years. Geo-Marine Letters 36, 281–291. https://link.springer.com/article/10.1007/s00367-016-0448-4.

Wang, S., Lü, H., Liu, J., Negendank, J.F.W., 2007. The early Holocene optimum inferred from a high-resolution pollen record of Huguangyan Maar Lake in southern China. Chinese. Sci. Bull. 52, 2829–2836. http://dx.doi.org/10.1007/s11434-007-0419-2.

Wang, X.L., Zhai, P.M., 2008. Changes in China's precipitation in various categories during 1957–2004. J. Trop. Meteorol. 24, 459–466 (in Chinese with English abstract). http://dx.doi.org/10.3969/j.issn.1004-4965.2008.05.003.

Wang, Y., Cheng, H., Edwards, R.L., He, Y., Kong, X., An, Z., Wu, J., Kelly, M.J., Dykoski, C.A., Li, X., 2005. The Holocene Asian monsoon: links to solar changes and North Atlantic climate. Science 308, 854–857. https://doi.org/10.1126/science.1106296.

Wu, Y., Wu, S.-Y., Wen, J., Xu, M., Tan, J., 2016. Changing characteristics of precipitation in China during 1960-2012. Int. J. Climatol. 36, 1387–1402. https://doi.org/10.1002/joc.4432.

Xiang, R., Sun, Y., Li, T., Oppo, D., Chen, M., Zheng, F., 2007. Paleoenvironmental change in the middle Okinawa Trough since the last deglaciation: Evidence from the sedimentation rate and planktonic foraminiferal record. Palaeogeogr. Palaeoclimatol.

Palaeoecol. 243, 378–393. https://doi.org/10.1016/j.palaeo.2006.08.016.

Xie, S., Evershed, R.P., Huang, X., Zhu, Z., Pancost, R.D., Meyers, P.A., Gong, L., Hu, C., Huang, J., Zhang, S., Gu, Y., Zhu, J., 2013. Concordant monsoon-driven postglacial hydrological changes in peat and stalagmite records and their impacts on prehistoric cultures in central China. Geology 41, 827–830. https://doi.org/10.1130/G34318.1.

Yang, X., Yang, H., Wang, B., Huang, L.-J., Shen, C.-C., Edwards, R.L., Cheng, H., 2019. Early-Holocene monsoon instability and climatic optimum recorded by Chinese stalagmites. Holocene 29, 1059–1067. https://doi.org/10.1177/0959683619831433.

Yang, Y., Yang, R., Cao, J., Zhao, J., Cheng, H., Wang, J., 2019. Relationship between the Asian summer monsoon circulation and speleothem $\delta^{18}O$ of Xiaobailong cave. Clim. Dyn. 53, 6351–6362. https://link.springer.com/article/10.1007/s00382-019-04935-6.

Yu, H., Liu, Z., Berné, S., Jia, G., Xiong, Y., Dickens, G.R., Wei, G., Shi, X., Liu, J.P., Chen, F., 2009. Variations in temperature and salinity of the surface water above the middle Okinawa Trough during the past 37kyr. Palaeogeogr. Palaeoclimatol. Palaeoecol. 281, 154–164. https://doi.org/10.1016/j.palaeo.2009.08.002.

Yuan, D., Cheng, H., Edwards, R.L., Dykoski, C.A., Kelly, M.J., Zhang, M., Qing, J., Lin, Y., Wang, Y., Wu, J., Dorale, J.A., An, Z., Cai, Y., 2004. Timing, duration, and transitions of the last interglacial Asian monsoon. Science 304, 575–578. https://doi.org/10.1126/science.1091220.

Zhang, H., Griffiths, M.L., Chiang, J.C.H., Kong, W., Wu, S., Atwood, A., Huang, J., Cheng, H., Ning, Y., Xie, S., 2018. East Asian hydroclimate modulated by the position of the westerlies during Termination I. Science 362, 580–583. https://doi.org/10.1126/science.aat9393.

Zhu, C., Yu, S., Lu, C., 1997. The study of Holocene environmental archaeology and extreme flood disaster in the Three Gorges of the Changjiang River and the Jianghan Plain. Acta Geol. Sin. 52(3), 268–277. https://doi.org/10.11821/xb199703009.

Zhu, Z., Feinberg, J.M., Xie, S., Bourne, M.D., Huang, C., Hu, C., Cheng, H., 2017. Holocene ENSO-related cyclic storms recorded by magnetic minerals in speleothems of central China. PNAS 114, 852–857. https://doi.org/10.1073/pnas.1610930114.

Zong, Y., Lloyd, J.M., Leng, M.J., Yim, W.W.-S., Huang, G., 2006. Reconstruction of Holocene monsoon history from the Pearl River Estuary, southern China, using diatoms and carbon isotope ratios. Holocene 16, 251–263. https://doi.org/10.1191/0959683606hl911rp.

Zweng, M.M., Reagan, J.R., Seidov, D., Boyer, T.P., Locarnini, R.A., Garcia, H.E., Mishonov, A.V., Baranova, O.K., Weathers, K., Paver, C.R., Smolyar, I., 2018. World Ocean Atlas 2018, vol 2: Salinity. A. Mishonov Technical Ed.; NOAA Atlas NESDIS 82

Figure captions

Fig. 1 The modern oceanic circulation system in the Okinawa Trough and locations of sediment cores referenced in the text. CCC, China Coastal Current; TWC, Taiwan Warm Current. Lower panels show July sea-surface temperature (SST) and July sea-surface salinity (SSS) based on the World Ocean Atlas 2018 (Locarnini et al. 2018; Zweng et al. 2018)

Fig. 2 (A) The reconstructed SSS record of core MD05-2908 from the southern OT, and the grey shaded area represent uncertainties of SSS reconstruction. (B) Stalagmite $\delta^{18}O$ record from Dongge Cave in southeast China (Dykoski et al., 2005). (C) The running correlation coefficient between SSS and stalagmite $\delta^{18}O$ values from Dongge Cave, a proxy for past EASM intensity.

Fig. 3 Results of time series analysis of the reconstructed SSS record from the

southern OT. (A) EEMD of the reconstructed SSS. (B) Spectral analysis results of the sum of c2–6. (C) Continuous wavelet power of the sum of c2–6. EEMD, ensemble empirical mode decomposition.

Fig. 4 The reconstructed SSS (psu) of core MD05-2908 (A; this study), core OKT-3 (B; Wang et al., 2016), core MD012404 (C; Chen et al., 2010), core A7 (D; Sun et al., 2005) and core KY07-04-01 (E; Kubota et al., 2010) from south to north. The dashed line shows the relative abundance of coastal water diatoms (%) in core MD05-2908.

Fig. 5 (A) Correlation coefficients between the EASM index and SSS (https://www.ecmwf.int/en/forecasts/dataset/ocean-reanalysis-system-5) in the East China Sea. (B) Correlation coefficients between the EASM index and summer mean precipitation (https://www.ecmwf.int/en/forecasts/datasets/reanalysis-datasets/era5) in the southern and central part of the larger East China Sea region.

Fig. 6 Summer precipitation records from South China and central-eastern China, and their asynchronous responses to the weakening of the EASM and solar insolation since the mid-Holocene. (A) Stalagmite $\delta^{18}O$ record from Dongge Cave in southeast China (Dykoski et al., 2005). (B) Solar insolation at 25 °N (average of June, July, August). (C) Stacked stalagmite $\delta^{18}O$ record for China (Yang et al., 2019). (D) Precipitation index for southern China (Ran and Feng, 2013). (E) Precipitation index from the Pearl River Estuary, southeastern China (Strong et al., 2013). (F)

Precipitation index from the Toushe Basin, Taiwan (Huang et al., 2020). (G) Moisture index from Huguangyan Maar Lake, South China (Wang et al., 2007). (H) Precipitation index for central China (Zhu et al., 2017). (I) Precipitation trend for central-eastern China based on different climate simulations (Dallmeyer et al., 2015).

Declaration of interests

☒ The authors declare that they have no known competing financial interests or personal relationships that could have appeared to influence the work reported in this paper.

☐ The authors declare the following financial interests/personal relationships which may be considered as potential competing interests:

Highlights

- Increasing SSS in the southern OT consistent with weakening EASM during the mid-Holocene
- Regional patterns of SSS with differences between the southern and northern OT
- Asynchronous summer precipitation patterns in southeastern and central eastern China
- The regional EASM precipitation is indeed a determinant parameter of SSS for the OT

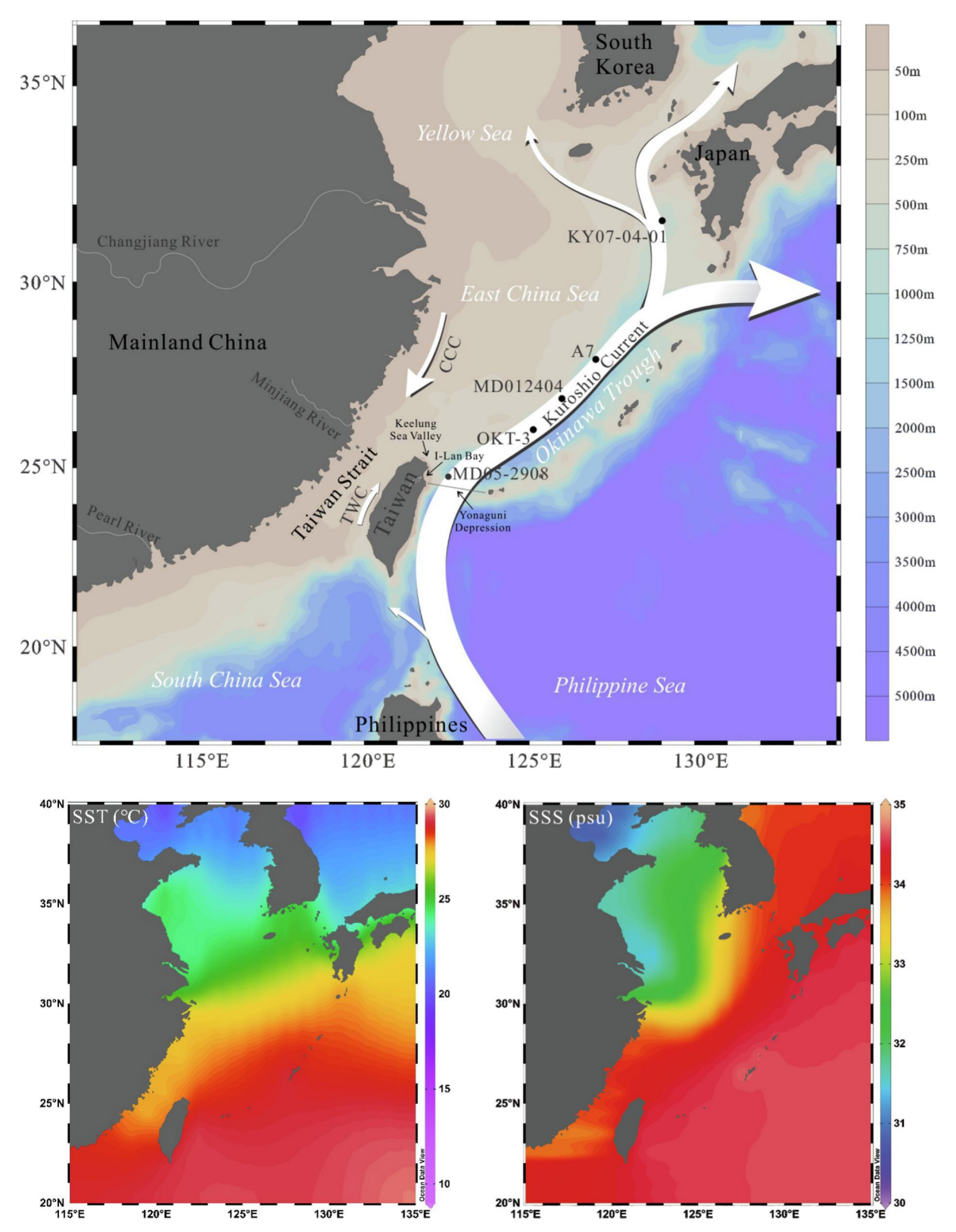
South Korea
Yellow Sea
Japan
KY07-04-01
East China Sea
Changjiang River
Mainland China
CCC
A7
Kuroshio Current
MD012404
Okinawa Trough
Minjiang River
Keelung Sea Valley
OKT-3
I-Lan Bay
MD05-2908
Taiwan Strait
TWC
Taiwan
Yonaguni Depression
Pearl River
South China Sea
Philippine Sea
Philippines
35°N
30°N
25°N
20°N
115°E
120°E
125°E
130°E
50m
100m
250m
500m
750m
1000m
1250m
1500m
2000m
2500m
3000m
3500m
4000m
4500m
5000m

SST (°C)
40°N
35°N
30°N
25°N
20°N
115°E
120°E
125°E
130°E
135°E
30
25
20
15
10
Ocean Data View

SSS (psu)
40°N
35°N
30°N
25°N
20°N
115°E
120°E
125°E
130°E
135°E
35
34
33
32
31
30
Ocean Data View

Figure 1

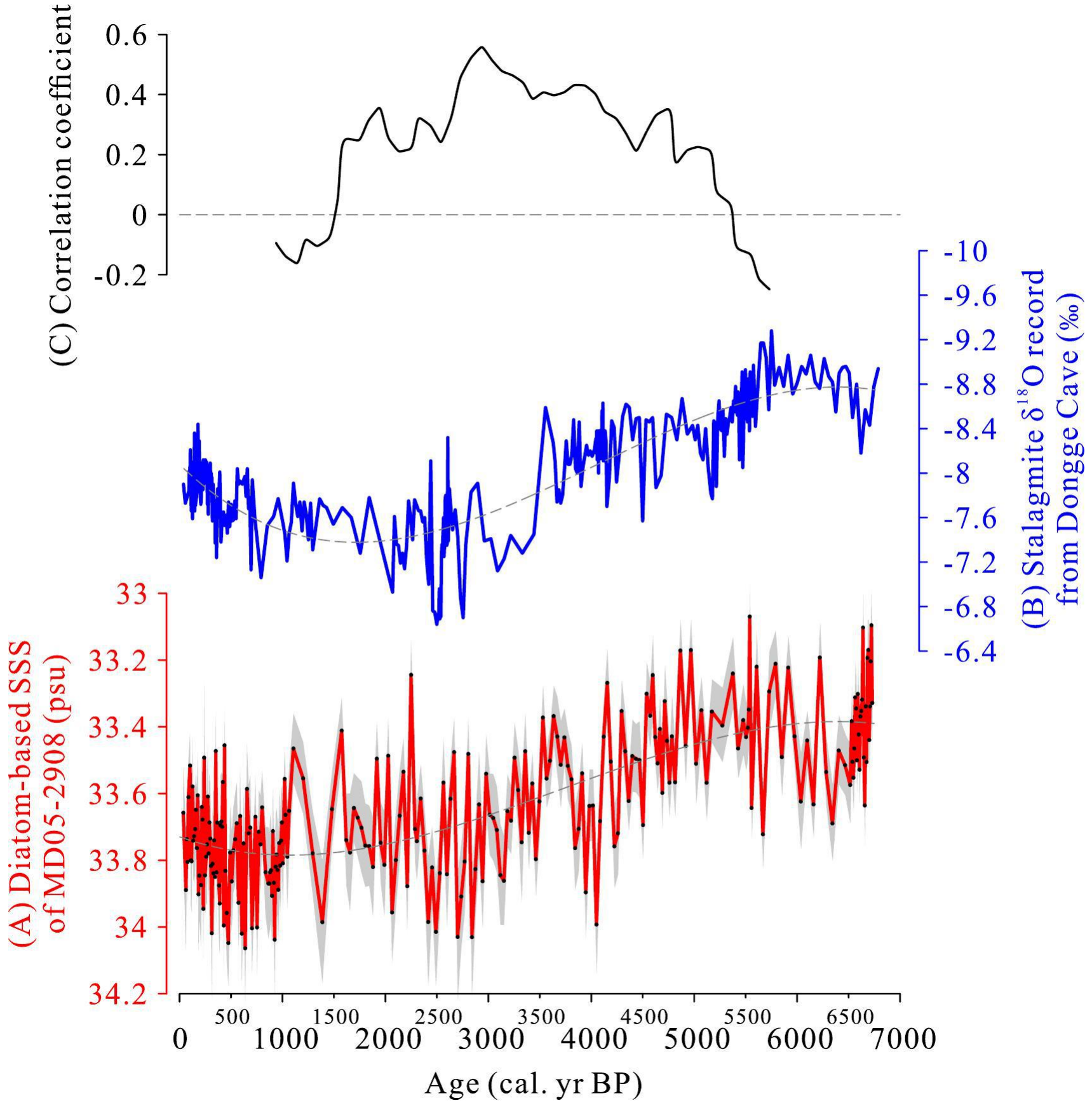
(C) Correlation coefficient
0.6
0.4
0.2
0
-0.2
(B) Stalagmite δ18O record from Dongge Cave (‰)
-10
-9.6
-9.2
-8.8
-8.4
-8
-7.6
-7.2
-6.8
-6.4
(A) Diatom-based SSS of MD05-2908 (psu)
33
33.2
33.4
33.6
33.8
34
34.2
500
1500
2500
3500
4500
5500
6500
0
1000
2000
3000
4000
5000
6000
7000
Age (cal. yr BP)

Figure 2

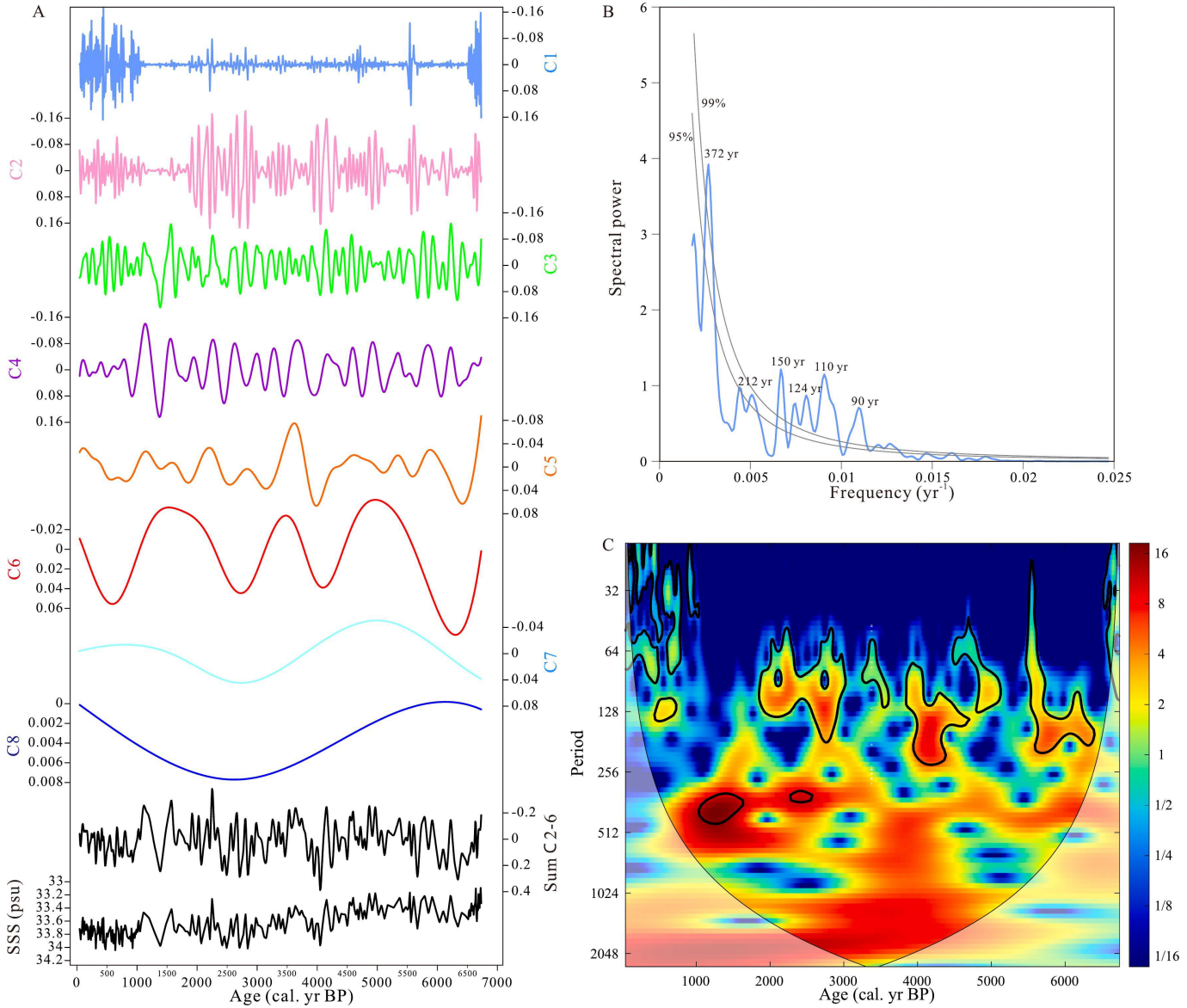
A
C1
C2
C3
C4
C5
C6
C7
C8
Sum C 2-6
SSS (psu)
Age (cal. yr BP)
B
Spectral power
Frequency (yr-1)
99%
95%
372 yr
212 yr
150 yr
124 yr
110 yr
90 yr
C
Period
Age (cal. yr BP)

Figure 3

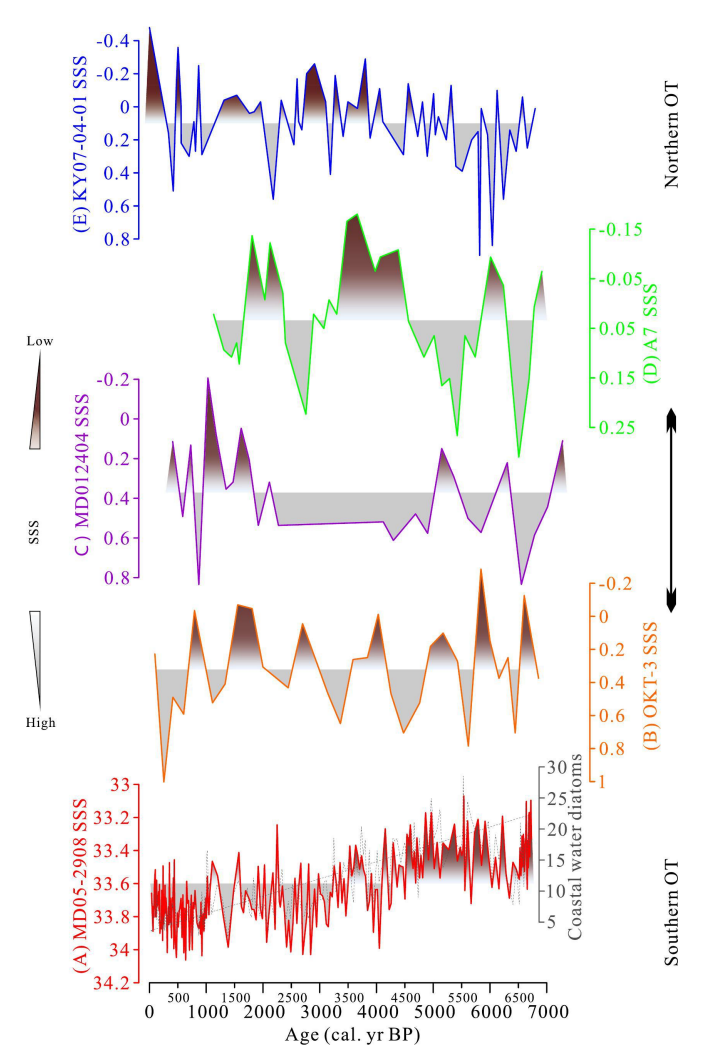
(E) KY07-04-01 SSS
-0.4
-0.2
0
0.2
0.4
0.6
0.8
Northern OT
-0.15
-0.05
0.05
0.15
0.25
(D) A7 SSS
Low
SSS
High
C) MD012404 SSS
-0.2
0
0.2
0.4
0.6
0.8
-0.2
0
0.2
0.4
0.6
0.8
1
(B) OKT-3 SSS
(A) MD05-2908 SSS
33
33.2
33.4
33.6
33.8
34
34.2
30
25
20
15
10
5
Coastal water diatoms
Southern OT
500
1500
2500
3500
4500
5500
6500
0
1000
2000
3000
4000
5000
6000
7000
Age (cal. yr BP)

Figure 4

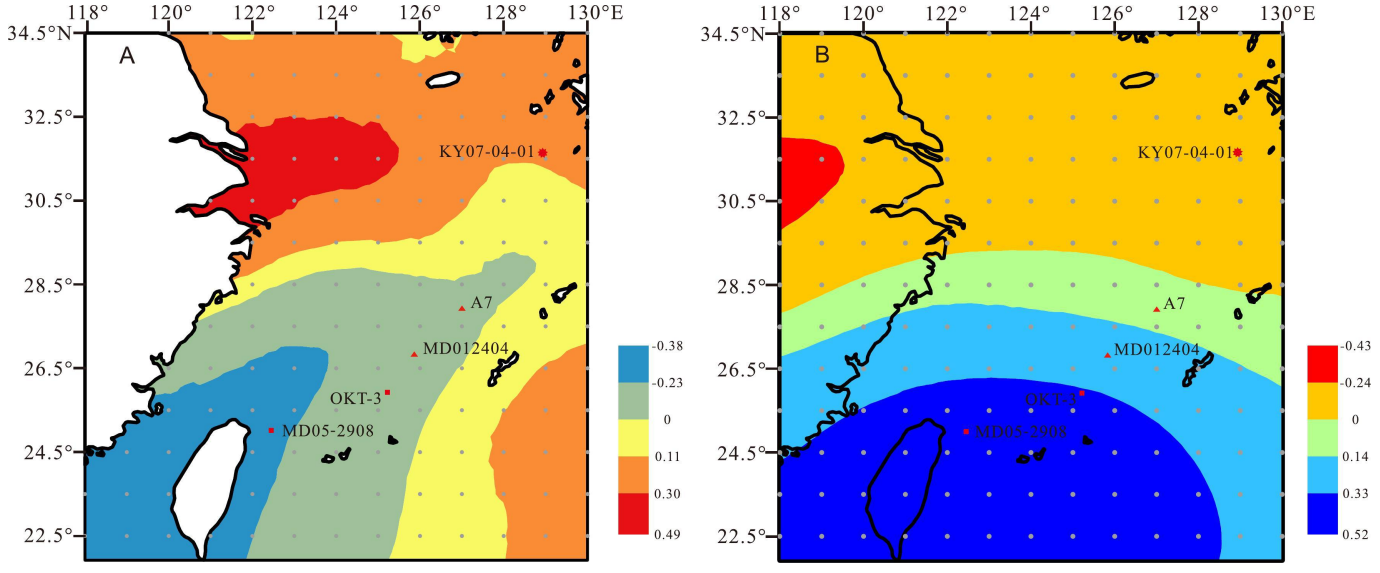
A
B
118°
120°
122°
124°
126°
128°
130°E
34.5°N
32.5°
30.5°
28.5°
26.5°
24.5°
22.5°
KY07-04-01
A7
MD012404
OKT-3
MD05-2908
-0.38
-0.23
0
0.11
0.30
0.49
-0.43
-0.24
0
0.14
0.33
0.52

Figure 5

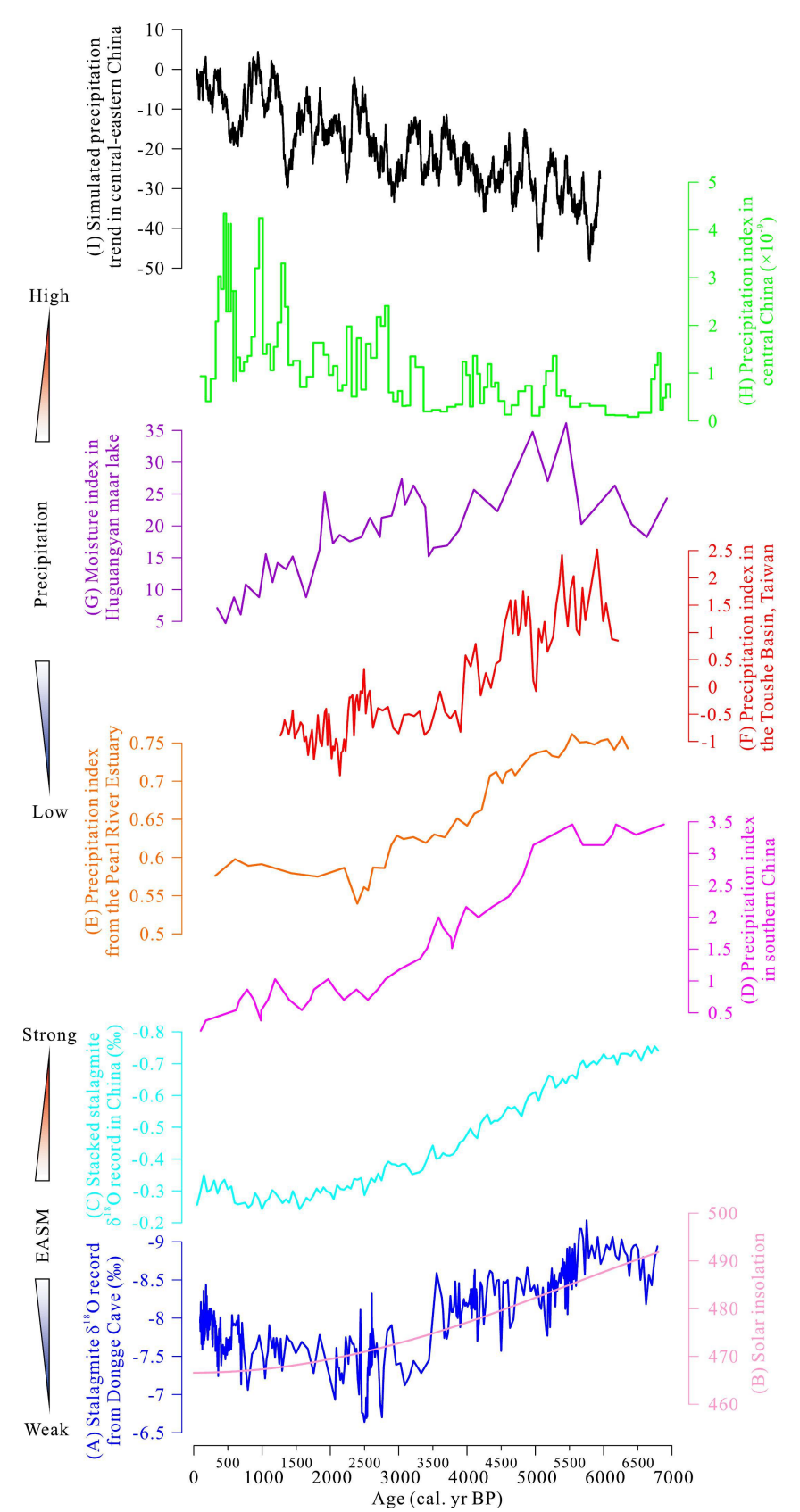
(I) Simulated precipitation trend in central-eastern China
(H) Precipitation index in central China (×10⁻⁹)
High
Precipitation
Low
(G) Moisture index in Huguangyan maar lake
(F) Precipitation index in the Toushe Basin, Taiwan
(E) Precipitation index from the Pearl River Estuary
(D) Precipitation index in southern China
Strong
EASM
Weak
(C) Stacked stalagmite δ18O record in China (‰)
(A) Stalagmite δ18O record from Dongge Cave (‰)
(B) Solar insolation
Age (cal. yr BP)

Figure 6